Closed-Form Approach to Rocket-Vehicles Aeroelastic Divergence

Dov Elyada*
Israel Armament Development Authority, Haifa, Israel

The aeroelastic divergence of a class of rocket-vehicle configurations is studied in closed form. The class is characterized by having the lateral aerodynamic loads distributed mainly about the vehicle nose and tail. The purpose is to demonstrate the feasibility of a closed-form approach and its usefulness in pinpointing the essentials of, and lending insight into, the phenomenon. The equations of motion are first derived; then, a dynamic frequency-domain stability analysis is carried out, yielding simple formulae for the divergence dynamic pressure and generalized static margin. The predivergence short-period roots behavior is also found. Expressions are derived for the steady-state angle of attack, accelerations, aerodynamic loads, and elastic bending of a perfectly aligned vehicle at divergence and of a misaligned vehicle at predivergence. For application to actual cases, a method is developed by which actual aerodynamic distributions may be converted into a form admissible to the theory. Validity is confirmed by comparison of results with those of a more exact theory and with available experimental data.

Nomenclature

$A_{11}, A_{12}, A_{21}, A_{22}$ = coefficients, defined by Eqs. (11)
A, B, C = coefficients, defined by Eqs. (15)
$c_{l_\alpha}(x)$ = vehicle lift-slope distribution, Fig. 2
$C_{L_\alpha}, C_{M_\alpha}, C_{M_q}$ = rigid-vehicle aerodynamic derivatives, Eqs. (5)
$C_{L_{\alpha_N}}, C_{T_{\alpha_T}}$ = lift-slope coefficients of L_N, L_T
c_N, c_T = lift fractions, defined by Eqs. (7g,h)
$(EI)_r$ = reference beam bending stiffness
$g_{11}, g_{12}, g_{21}, g_{22}$ = inertia-flexibility influence coefficients; Eq. (4)
h_0, h = rigid and generalized static margins; Eqs. (7d), (18)
I = rigid vehicle lateral moment of inertia around CG
j_0^2 = nondimensional moment of inertia; Eq. (7b)
$K_n, n = 0 \ldots 3$ = nth-order moment of the lift-slope distribution; Eq. (28)
L = vehicle total lift force
L_N, L_T = nose and tail concentrated lift forces; Fig. 3
l, l_e = aerodynamic and overall vehicle lengths; Fig. 2
l_N, l_T = nose and tail lever arms; Fig. 2
M = vehicle total pitching moment around CG
$m, m'(x)$ = vehicle total mass and mass distribution function
Q, q = dynamic pressure, $\rho U^2/2$, and nondimensional; Eq. (7i)
r_0^2 = constant, defined by Eq. (7c)
S_r = vehicle aerodynamic reference area
$s, s^{(1)}, s^{(2)}$ = Laplace's variable and roots of Eq. (14)
U = vehicle speed, flow speed; Fig. 3
$w(x)$ = vehicle deformation function; Fig. 3
x = coordinate axis along the rigid line; Figs. 2 and 3
x_N, x_T, x_{cp}, x_{cg} = x-coordinates of points N, T, CP, CG; Fig. 2
α = rigid line angle of attack; Fig. 3
γ = flight-path inclination; Fig. 3
$\gamma_{11}, \gamma_{12}, \gamma_{21}, \gamma_{22}$ = nondimensional $g_{11}, g_{12}, g_{21}, g_{22}$; Eq. (7k)
η = nondimensional lateral acceleration; Eq. (10a)
θ = Body angle of the rigid line; Fig. 3
λ_N, λ_T = nondimensional nose and tail lever arms; Eqs. (7e,f)
μ = mass ratio, vehicle/air; Eq. (7a)
ξ, ζ = wind axes, Fig. 3
σ = aerodynamic "standard deviation"; Eq. (31)
$\phi_N, \phi_T, \{\phi\}$ = elastic increments of nose and tail local angles of attack; Fig. 3
χ = nondimensional pitch rate; Eq. (10b)
ψ_N, ψ_T = misalignment increments of nose and tail local angles of attack
Ω = short-period mode angular frequency
$()^\bullet$ = derivative with respect to time
$()^*$ = derivative with respect to nondimensional time; Eq. (7j)
$\overline{()}$ = Laplace-transformed variable

Subscripts

D = at discriminant vanishing; Fig. 4
div = at divergence stability boundary
h = at vanishing of the generalized static margin
N, T = of nose point, tail point, respectively
0 = of initial conditions
∞ = at steady state

Received June 30, 1987; revision received April 29, 1988.

*Senior Research Scientist and Head, Structures Section. Member AIAA.

Introduction

BY "Rocket-Vehicle Aeroelastic Divergence (ROVALD)" we refer to a nonoscillatory instability involving, in a closed loop, the vehicle angle of attack, lateral acceleration, structural bending and loss of static margin. It usually

leads to structural failure[1,2] and, in any case, to undesirable effects such as trajectory errors and roll-resonance.[2,3] The closed-loop mechanism and its effects are depicted in Fig. 1. Its stability and severity of effects strongly depend on the flight dynamic pressure. Though ROVALD is inherent in unguided, very slender configurations such as sounding rockets,[1-3] it is by no means absent from slender guided missiles, launch vehicles, and certain flexible aircraft configurations. In the latter group it is usually absorbed in the general aero-servo-elasticity problem.

Several relatively elaborate numerically based procedures for calculating ROVALD have been developed in the past. References 4–9 are examples dealing with nonrolling vehicles. However, whereas in other aeroelastic fields, e.g., wing divergence and flutter, simple "textbook" models have been devised – for purposes of instruction as well as for "back of the envelope" estimations – ROVALD seems to have missed this kind of approach. A probable reason: it is not quite obvious how to make the structural side of the problem statically determinate, a feature that seems imperative in such analyses. In this paper we demonstrate that, provided the aerodynamic configuration cooperates, this is indeed possible. Consequently, a theory of ROVALD is developed in closed form, yielding remarkably simple yet reasonably accurate expressions. Nevertheless, it is not our purpose here to compete for accuracy with more general numerical schemes. Rather, the work is intended to shed light on the physical essentials of ROVALD, while the relative accuracy obtained is looked upon as a confirmation of getting these essentials right.

The aerodynamic configuration we focus upon consists of a nose cone or ogive, a slender cylindrical body, and a system of tail fins. In such configurations (Fig. 2), lift is distributed mainly on the nose and tail and is naturally idealized into a pair of concentrated forces: a nose force and a tail force. For brevity we will refer to such configurations as "2L."

The key idea making the closed-form approach possible lies in regarding the two concentrated lifts as *support reactions* of a statically determinate bending beam representing the vehicle structure. The beam is loaded by distributed inertial loads, resulting from only two rigid-body modes of lateral acceleration – the effect of higher modes neglected. The aeroelastic loop is closed by letting the motion in the two modes be determined by the two lifts through rigid-body relations.

After deriving the vehicle aeroelastic equations of motion, a dynamic, frequency-domain stability analysis is carried out, resulting in expressions for the divergence dynamic pressure and the generalized static margin, and revealing the prediver-gence short-period roots. The steady-state behavior of a diverging perfectly aligned vehicle and a predivergent misaligned vehicle is then investigated. Finally, a method is developed that converts distributed lifts into equivalent systems of two concentrated forces. Using this method comparisons are made with results of a more exact theory for some rather realistic cases. Comparison with actual ROVALD data is also presented.

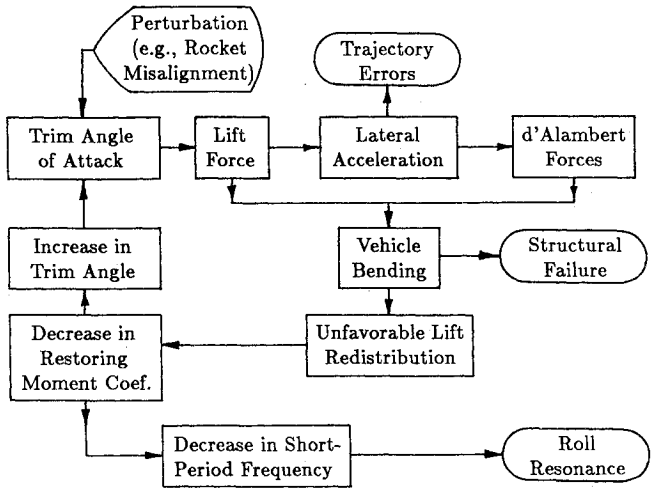

Fig. 1 Rocket vehicles aeroelastic divergence—mechanism and effects.

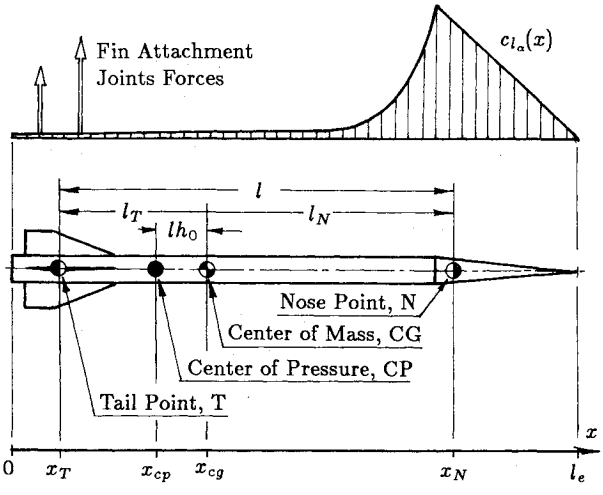

Fig. 2 A "2L" configuration, typical aerodynamic lift-slope distribution and related geometrical quanities.

Equations of Motion

Let a slender, flexible, unguided, nonrolling, 2L-configured rocket vehicle be given. Let the lift distribution be approximated by two concentrated forces as shown in Fig. 3. The points of application of the forward and aft forces will be called the *nose point* (N) and the *tail point* (T), respectively. These, together with related geometrical properties, are shown in Fig. 2. The distance between points N and T, denoted by l, will be called the *aerodynamic length* of the vehicle and will serve as a typical length of the problem.

We shall proceed to derive the two-degrees-of-freedom short-period mode equations, as influenced by the vehicle flexibility. In this we shall assume the following:

1) The motion and elastic deflection of the vehicle, and the forces acting on it, are contained in the "vertical" plane.

2) The only external forces acting on the vehicle are the aerodynamic lift forces. Thrust, drag, and gravitation are absent. The aerodynamic forces are quasisteady and proportional to the *local effective* (small) angle of attack at their respective points of application.

3) Structurally, the vehicle is considered a simple, nonuniform bending beam represented by an elastic axis. Deflections and slopes are assumed small. The mass is regarded as distributed on, and rigidly attached to, the elastic axis.

4) The accelerations associated with deformation are negligible compared to the ones connected with rigid-body motion. (For this to be true, the frequency response band of the first free-free bending mode must be higher than, and well separated from, that of the short-period rigid-body mode.)

If assumption 4 is to be meaningful, it is necessary to specify how the motion of a vehicle point-mass is partitioned into rigid-body and elastic constituents, an operation otherwise quite ambiguous. To this end we define the *rigid line,* an imaginary straight line passing through points N and T on the deformed elastic axis, and agree to measure deformation relative to it. The "rigid-body motion" is thus the motion of the rigid line. The perturbed vehicle, the rigid line, and related quantities are shown in Fig. 3.

We choose as a reference frame the inertial wind axes ξ,ζ (Fig. 3), which, at the time-of-interest t_0 happen to possess the instantaneous vehicle vector-velocity, with the ξ-axis pointing

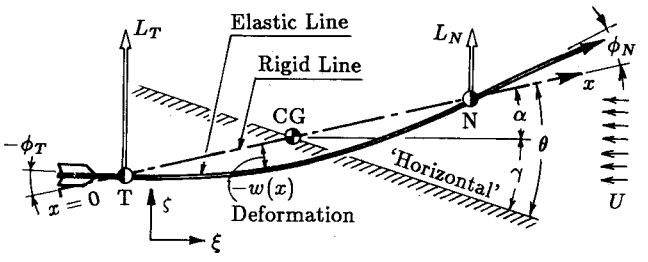

Fig. 3 The perturbed vehicle, reference frame, displacement partition, rigid and elastic DOF and aerodynamic loads.

in the direction of that velocity. Disturbance of the vehicle produces only minute changes in the magnitude U of that velocity; hence we take $U = \text{const}$. The two degrees of freedom describing the rigid line motion are chosen as γ, the inclination of the flight path of the center of mass projection on the rigid line, and θ, the body angle of the rigid line. The rigid line angle of attack, $\alpha = \theta - \gamma$, is assumed small. Also shown in Fig. 3 are ϕ_N and ϕ_T, the elastic increments of the *local* angles of attack at points N and T, respectively.

A consequence of assumption 4 is that the equations of motion of the rigid line are the same as those of the vehicle itself regarded as rigid. Let m be the vehicle mass, I its lateral, around-CG moment of inertia, then

$$\begin{Bmatrix} L \\ M \end{Bmatrix} = \begin{bmatrix} m & 0 \\ 0 & I \end{bmatrix} \begin{Bmatrix} U\dot{\gamma} \\ \ddot{\theta} \end{Bmatrix} \tag{1}$$

L, the total lift, and M, the total pitching moment around CG, are related to the nose and tail lifts L_N, L_T, and to their respective lever arms l_N, l_T, (Fig. 2) as follows:

$$\begin{Bmatrix} L \\ M \end{Bmatrix} = \begin{bmatrix} 1 & 1 \\ l_N & -l_T \end{bmatrix} \begin{Bmatrix} L_N \\ L_T \end{Bmatrix} \tag{2}$$

Next is the matrix form of the aerodynamic forces as determined by assumption 2,

$$\begin{Bmatrix} L_N \\ L_T \end{Bmatrix} = QS_r \begin{bmatrix} C_{L\alpha_N} & 0 \\ 0 & C_{L\alpha_T} \end{bmatrix} \left(\begin{bmatrix} 1 & -l_N \\ 1 & l_T \end{bmatrix} \begin{Bmatrix} \alpha \\ \dot{\theta}/U \end{Bmatrix} \begin{Bmatrix} \phi_N \\ \phi_T \end{Bmatrix} \right) \tag{3}$$

where Q is the dynamic pressure, S_r the aerodynamic reference area, and $C_{L\alpha_N}$, $C_{L\alpha_T}$ the lift-slope coefficients associated with L_N, L_T, respectively.

For expressing the vehicle elastic properties we replace ad hoc our reference frame by one which is fixed to the rigid line. This frame is, in general, noninertial, wherein point-masses appear loaded by apparent d'Alambert forces linear in the frame acceleration parameters $U\dot{\gamma}$ and $\ddot{\theta}$. Relative to this frame the picture is that of a statically determinate bending beam, simply supported at points N and T, loaded exclusively by the above d'Alambert forces and having L_N and L_T for support reactions. The resulting beam deflection, which by assumption 4 is quasistatic, [hence the absence, in Eq. (4), of time derivatives of ϕ_N and ϕ_T] can be regarded as a direct consequence of $U\dot{\gamma}$ and $\ddot{\theta}$, and its features of interest expressed as

$$\begin{Bmatrix} \phi_N \\ \phi_T \end{Bmatrix} = \begin{bmatrix} g_{11} & g_{12} \\ g_{21} & g_{22} \end{bmatrix} \begin{Bmatrix} U\dot{\gamma} \\ \ddot{\theta} \end{Bmatrix} \tag{4}$$

Appropriate influence coefficients g_{ij} are calculated as follows. Assume that in Fig. 3 the deflection $w(x)$ is a combination of two modes, numbered 1 and 2, caused by "downward" distributed loads $m'(x)$ and $(x - x_{cg})m'(x)$, respectively, $m'(x)$ being the vehicle mass distribution. Then

$$\begin{aligned} g_{11} &= \phi_N \text{ in mode 1}; \quad g_{12} = \phi_N \text{ in mode 2} \\ g_{21} &= \phi_T \text{ in mode 1}; \quad g_{22} = \phi_T \text{ in mode 2} \end{aligned} \tag{4a}$$

The equations of motion are now obtained by expressing all forces and deformations in terms of γ, θ, α, and their derivatives, using Eqs. (1-4). Define

$$C_{L_\alpha} \equiv \frac{\partial}{\partial \alpha}\left(\frac{L}{QS_r}\right) = C_{L\alpha_N} + C_{L\alpha_T} \tag{5a}$$

$$C_{M_\alpha} \equiv \frac{\partial}{\partial \alpha}\left(\frac{M}{QS_r l}\right) = \frac{l_N}{l} C_{L\alpha_N} - \frac{l_T}{l} C_{L\alpha_T} \tag{5b}$$

$$C_{M_q} \equiv \frac{\partial}{\partial (l\dot{\theta}/U)}\left(\frac{M}{QS_r l}\right) = -\left(\frac{l_N}{l}\right)^2 C_{L\alpha_N} - \left(\frac{l_T}{l}\right)^2 C_{L\alpha_T} \tag{5c}$$

The quantities C_{L_α}, C_{M_α}, and C_{M_q} are the conventional, rigid-vehicle lift, and pitching moment coefficient derivatives with respect to α and $\hat{q} \equiv l\dot{\theta}/U$. Note that in these definitions the reference lever-arm is the aerodynamic length l rather than the usual reference diameter. Using Eq. (5) we obtain

$$\left(\frac{1}{QS_r l^2 C_{L\alpha_N} C_{L\alpha_T}} \begin{bmatrix} -l^2 C_{M_q} & -l C_{M_\alpha} \\ -l C_{M_\alpha} & C_{L_\alpha} \end{bmatrix} \begin{bmatrix} m & 0 \\ 0 & I \end{bmatrix} - \frac{1}{l} \times \begin{bmatrix} l_T & l_N \\ 1 & -1 \end{bmatrix} \begin{bmatrix} g_{11} & g_{12} \\ g_{21} & g_{22} \end{bmatrix} \right) \begin{Bmatrix} U\dot{\gamma} \\ \ddot{\theta} \end{Bmatrix} + \begin{bmatrix} -1 & 0 \\ 0 & 1 \end{bmatrix} \begin{Bmatrix} \alpha \\ \dot{\theta}/U \end{Bmatrix} = \begin{Bmatrix} 0 \\ 0 \end{Bmatrix} \tag{6}$$

Let us introduce the following nondimensional quantities:

$$\mu \equiv m/(\rho S_r l) \quad \text{(mass ratio)} \tag{7a}$$

$$j_0^2 \equiv I/(ml^2) \tag{7b}$$

$$r_0^2 \equiv -C_{M_q}/C_{L_\alpha} \tag{7c}$$

$$h_0 \equiv -C_{M_\alpha}/C_{L_\alpha} \text{ (rigid static margin)} \tag{7d}$$

$$\lambda_N \equiv l_N/l \tag{7e}$$

$$\lambda_T \equiv l_T/l \tag{7f}$$

$$c_N \equiv C_{L\alpha_N}/C_{L_\alpha} \tag{7g}$$

$$c_T \equiv C_{L\alpha_T}/C_{L_\alpha} \tag{7h}$$

$$q \equiv QS_r l^2/(EI)_r$$

$$[(EI)_r = \text{reference beam stiffness}] \tag{7i}$$

$$()^* \equiv (l/U)()^\cdot \tag{7j}$$

$$\begin{bmatrix} \gamma_{11}\gamma_{12} \\ \gamma_{21}\gamma_{22} \end{bmatrix} \equiv \frac{(EI)_r}{ml^2} \begin{bmatrix} g_{11}g_{12}/l \\ g_{21}g_{22}/l \end{bmatrix} \tag{7k}$$

Using Eqs. (7), a nondimensional form of Eq. (6) is obtained:

$$2\mu \left(\frac{1}{c_N c_T C_{L_\alpha}} \begin{bmatrix} r_0^2 & h_0 \\ h_0 & 1 \end{bmatrix} \begin{bmatrix} 1 & 0 \\ 0 & j_0^2 \end{bmatrix} - q \begin{bmatrix} \lambda_T & \lambda_N \\ 1 & -1 \end{bmatrix} \times \begin{bmatrix} \lambda_{11} & \lambda_{12} \\ \lambda_{21} & \lambda_{22} \end{bmatrix} \right) \begin{Bmatrix} \lambda^* \\ \theta^{**} \end{Bmatrix} + \begin{bmatrix} -1 & 0 \\ 0 & 1 \end{bmatrix} \begin{Bmatrix} \alpha \\ \theta^* \end{Bmatrix} = \begin{Bmatrix} 0 \\ 0 \end{Bmatrix} \tag{8}$$

The term involving q expresses the influence of flexibility. Observe [Eq. (7i)] that besides being a nondimensional dynamic pressure, q is a measure of the ratio of aerodynamic to structural stiffnesses. Thus $q = 0$ marks the rigid-body limit as well as that of zero dynamic pressure.

To complete the system of equations we supplement Eq. (8) with $\lambda - \theta + \alpha = 0$ (Fig. 3) or, preferably, with

$$\gamma^* - \theta^* + \alpha^* = 0 \tag{9}$$

For brevity we define

$$\eta \equiv \gamma^* \quad \text{nondimensional lateral acceleration} \tag{10a}$$

$$\chi \equiv \theta^* \quad \text{nondimensional pitch rate} \tag{10b}$$

$$A_{11}(q) \equiv 2\mu\left[\frac{r_0^2}{c_N c_T C_{L_\alpha}} - q(\lambda_T\gamma_{11} + \lambda_N\gamma_{21})\right] \tag{11a}$$

$$A_{12}(q) \equiv 2\mu\left[\frac{h_0 j_0^2}{c_N c_T C_{L_\alpha}} - q(\lambda_T\gamma_{12} + \lambda_N\gamma_{22})\right] \tag{11b}$$

$$A_{21}(q) \equiv 2\mu\left[\frac{h_0}{c_N c_T C_{L_\alpha}} - q(\gamma_{11} - \gamma_{21})\right] \tag{11c}$$

$$A_{22}(q) \equiv 2\mu\left[\frac{j_0^2}{c_N c_T C_{L_\alpha}} - q(\gamma_{12} - \gamma_{22})\right] \tag{11d}$$

After some manipulation, Eqs. (8) and (9) are now expressed as

$$\left.\begin{aligned} A_{11}\eta + A_{12}\chi^* - \alpha &= 0 \\ (1+A_{21})\eta + A_{22}\chi^* + \alpha^* &= 0 \\ \eta - \chi + \alpha^* &= 0 \end{aligned}\right\} \tag{12}$$

which are the aeroelastic short-period mode equations used in this work.

Frequency-Domain Analysis

Consider a Laplace transform of Eq. (12), s denoting Laplace's variable and "bars" denoting transformed quantities. For stability analysis zero initial conditions are taken:

$$\begin{bmatrix} A_{11} & sA_{12} & -1 \\ 1 + A_{21} & sA_{22} & -s \\ 1 & -1 & s \end{bmatrix} \begin{Bmatrix} \bar{\eta}(s) \\ \bar{\chi}(s) \\ \bar{\alpha}(s) \end{Bmatrix} = \begin{Bmatrix} 0 \\ 0 \\ 0 \end{Bmatrix} \tag{13}$$

The characteristic equation takes the form

$$A(q)s^2 + B(q)s + C(q) = 0 \tag{14}$$

where

$$A(q) = A_{11}A_{22} - A_{12}A_{21} \tag{15a}$$

$$B(q) = A_{11} + A_{22} \tag{15b}$$

$$C(q) = 1 + A_{21} \tag{15c}$$

The roots of Eq. (14) represent stable motion (i.e., possess negative real parts) if and only if $A \neq 0$ and both B/A and C/A are positive (Routh's criterion). It turns out (Eqs. 15, 11, 7, and 5) that, for a vehicle designed to be statically stable as a rigid body, $A(0)$, $B(0)$, and $C(0)$ are all positive. The *actual* (least q) instability thus occurs, on increasing q, whenever any one of A, B, or C vanishes while the other two are still positive. The following cases might exist:

(i) $A = 0, \quad B > 0, \quad C > 0$
(ii) $A > 0, \quad B = 0, \quad C > 0$
(iii) $A > 0, \quad B > 0, \quad C = 0$

Cases (i) and (ii) are nonphysical; they involve unsteady acceleration ($s \neq 0$), thereby violating assumption 4. Fortunately, it has been shown elsewhere[10] that for "typical" 2L configurations their (mathematical) occurrence is quite unlikely. [The demonstration is based on numerous diverse examples and partly qualitative analysis: if "typical" means $\gamma_{11} > 0$, $\gamma_{21} < 0$, then, for either case (i) or (ii) to happen, the unlikely condition $(\gamma_{12} - \gamma_{22})/(\gamma_{11} - \gamma_{21}) \geq j_0^2/h_0$ must be satisfied.] Case (iii), on the other hand, does conform with the theoretical assumptions and is the rule in 2L's. Anticipating results to come, we refer to it as "divergence" (div).

Letting $C = 0$ in Eq. (14) we find the divergence roots,

$$s_{\text{div}}^{(1)} = 0, \qquad s_{\text{div}}^{(2)} = -(B/A)_{\text{div}} < 0 \tag{16a,b}$$

which, being real, show that divergence is nonoscillatory. The divergence dynamic pressure is readily obtained from Eqs. (15c, 11c):

$$q_{\text{div}} = \frac{1}{\gamma_{11} - \gamma_{21}}\left(\frac{h_0}{c_N c_T C_{L_\alpha}} + \frac{1}{2\mu}\right) \tag{17}$$

A common measure of static stability of (rigid) flight vehicles is the static margin, represented here by h_0. From examination of Eqs. (15c, 11c) an analogy with respect to their role in C can be seen to exist between h_0 of a rigid vehicle ($q = 0$) and the quantity

$$h = h_0 - q[c_N c_T C_{L_\alpha}(\gamma_{11} - \gamma_{21})] \tag{18}$$

of a flexible one. Equation (18) is therefore suggested as a natural definition of the *generalized static margin* (GSM), a prevalent[5] measure of *flexible* vehicles static stability.

The GSM is seen to vanish at a dynamic pressure q_h

$$q_h = \frac{h_0}{c_N c_T C_{L_\alpha}(\gamma_{11} - \gamma_{21})} \tag{19a}$$

$$\frac{q_{\text{div}}}{q_h} = 1 + \frac{c_N c_T C_{L_\alpha}}{h_0}\left(\frac{1}{2\mu}\right) \tag{19b}$$

which, for vehicles of reasonable h_0, is practically indistinguishable from q_{div}. This is so because μ is large; it is roughly the ratio of the vehicle mass to that of the air it displaces (Eq. 7a). Taking $q_{\text{div}} \simeq q_h$, the GSM can be expressed as follows:

$$h \simeq h_0(1 - Q/Q_{\text{div}}) \tag{20}$$

Provided the linearity-in-Q is carried over, this form is not restricted to vehicles of the 2L variety, or to static margins based on l. As such, it may serve as quite a general definition of the GSM.

Another distinguished q is q_D, for which the short-period mode frequency just vanishes. It is determined by the condition $B^2 - 4AC = 0$, leading to

$$\frac{q_D}{q_h} \simeq 1 - \left(\frac{(A_{11} - A_{22})^2}{4A}\right)_D \frac{c_N c_T C_{L_\alpha}}{h_0}\left(\frac{1}{2\mu}\right) \tag{21a}$$

$$s_D^{(1)} = s_D^{(2)} \simeq (-B/2A)_{\text{div}} = s_{\text{div}}^{(2)}/2 \tag{21b}$$

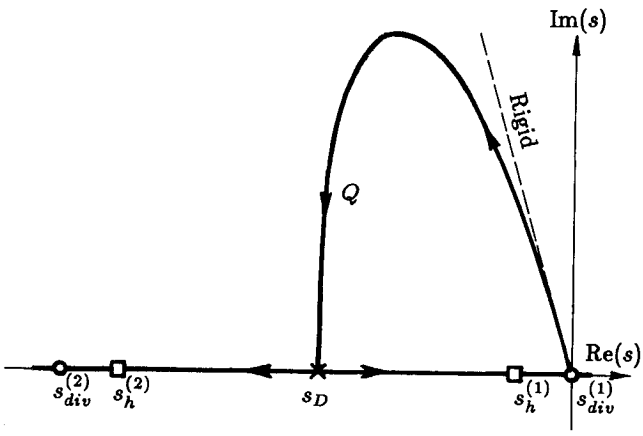

Fig. 4 Short-period mode root-locus, qualitative.

Again, for reasonable-h_0 vehicles, q_D is very close to q_h (and to q_{div}). In general, $q_D < q_h < q_{\text{div}}$ (Fig. 4).

The small discrepancies between q_D, q_h and q_{div} can be traced to aerodynamic damping, making the vehicle dynamically stable even when statically slightly unstable, and making its motion nonoscillatory even when h (a factor in the aerodynamic "spring constant") is still positive. For practical purposes, however, one may take $q_D = q_h = q_{\text{div}}$.

For $q < q_D$ the approximate ($\mu \gg 1$) short-period mode *dimensional* frequency is $\Omega = (U/l, \sqrt{C/A}$, or

$$\Omega^2 = \frac{4\mu h_0}{\rho l^2 c_N c_T C_{L_\alpha}} \frac{Q}{A(Q)} \left(1 - \frac{Q}{Q_D}\right) \tag{22}$$

We see that Ω vanishes at $Q = 0$ and $Q = Q_D$ and has a maximum somewhere in between (Fig. 4). Consequently, Ω is always less than that of the associated rigid vehicle ($Q_D \to \infty$). Thus, in a vehicle designed to roll at a frequency smaller than its rigid Ω, failure to consider this may result in an unexpected roll resonance. Finally, we recall that, by assumption 4, excessive proximity of Ω to the first bending mode frequency may affect the accuracy of Eq. (22).

Divergence Steady-State Motion

Let in Eq. (13) $1 + A_{21} = 0$ (divergence), add the initial condition terms and rewrite as follows:

$$\begin{bmatrix} A_{11} & sA_{12} & -1 \\ 0 & A_{22} & 1 \\ 1 & -1 & s \end{bmatrix} \begin{Bmatrix} s\bar{\eta}(s) \\ s\bar{\chi}(s) \\ s\bar{\alpha}(s) \end{Bmatrix} = \begin{Bmatrix} sA_{12}\chi_0 \\ A_{22}\chi_0 + \alpha_0 \\ s\alpha_0 \end{Bmatrix} \tag{23}$$

where the subscript "0" denotes initial state. The steady-state motion is now readily obtained using the Laplace transform final value theorem, $\lim_{t\to\infty} f(t) = \lim_{s\to 0} s\bar{f}(s)$:

$$\begin{bmatrix} A_{11} & 0 & -1 \\ 0 & A_{22} & 1 \\ 1 & -1 & 0 \end{bmatrix} \begin{Bmatrix} \eta_\infty \\ \chi_\infty \\ \alpha_\infty \end{Bmatrix} = \begin{Bmatrix} 0 \\ A_{22}\chi_0 + \alpha_0 \\ 0 \end{Bmatrix} \tag{24}$$

which leads† to the following features of interest:

$$\alpha_{\infty,\text{div}} = \text{const} = A_{11}(A_{22}\chi_0 + \alpha_0)/B \tag{25a}$$

$$\ddot{\theta}_{\infty,\text{div}} = 0 \tag{25b}$$

$$M_{\infty,\text{div}} = 0 \tag{25c}$$

$$(U\dot{\gamma})_{\infty,\text{div}} = (U\dot{\theta})_{\infty,\text{div}}$$

$$= \alpha_\infty h_0/(\lambda_N c_N g_{11} - \lambda_T c_T g_{21}) \tag{25d}$$

$$(L_N/L)_{\infty,\text{div}} = \lambda_T \tag{25e}$$

$$(L_T/L)_{\infty,\text{div}} = \lambda_N \tag{25f}$$

$$(C_{L_\alpha})_{\text{div}}/(C_{L_\alpha})_{\text{rigid}} = c_N c_T(\gamma_{11} - \gamma_{21})/(\gamma_N c_N \gamma_{11} - \gamma_T c_T \gamma_{21}) \tag{25g}$$

$$\begin{Bmatrix} \phi_N \\ \phi_T \end{Bmatrix}_{\infty,\text{div}} = \frac{\alpha_\infty h_0}{\lambda_N c_N \gamma_{11} - \lambda_T c_T \gamma_{21}} \begin{bmatrix} \gamma_{11} \\ \gamma_{21} \end{bmatrix} \tag{25h}$$

$w(x)$ consists of mode 1 only. Thus, at divergence, the vehicle flies just as a rigid-bent one would: with a constant, trimmed angle of attack and a constant rate of turn. Its deformation shape is then pure mode 1 [see Eq. (4a)]. The amount of response is determined by the strength of the initial disturbance. Note that because $\{\phi\}$ is constant, the results, Eqs. (25), are in good accord with assumption 4.

Effects of Aerodynamic Misalignment

In the sense of this work, a vehicle is aerodynamically misaligned if in the unstressed state its elastic line forms nonvanishing angles, ψ_N, ψ_T, at points N and T, respectively, with the rigid line. The symbols ψ_N, ψ_T are nonelastic counterparts of ϕ_N, ϕ_T. The misaligned vehicle equations of motion are

$$\left.\begin{aligned} A_{11}\eta + A_{12}\chi^* - \alpha &= \lambda_T\psi_N + \lambda_N\psi_T \\ (1 + A_{21})\eta + A_{22}\chi^* + \alpha^* &= \psi_N - \psi_T \\ \eta - \chi + \alpha^* &= 0 \end{aligned}\right\} \tag{26}$$

Repeating previous-section steps, only with $1 + A_{21} \neq 0$, the misaligned vehicle predivergence behavior is found to be

$$\alpha_\infty = \text{const} = \frac{\psi_N - \psi_T}{2\mu(\gamma_{11} - \gamma_{21})} \cdot \frac{A_{11}(q)/q_{\text{div}}}{1 - q/q_{\text{div}}} - (\lambda_T\psi_N + \lambda_N\psi_T) \tag{27a}$$

$$\ddot{\theta}_\infty = 0 \tag{27b}$$

$$M_\infty = 0 \tag{27c}$$

$$(U\dot{\gamma})_\infty = (U\dot{\theta})_\infty = \frac{\psi_N - \psi_T}{g_{11} - g_{21}} \cdot \frac{Q/Q_{\text{div}}}{1 - Q/Q_{\text{div}}} \tag{27d}$$

All actual vehicles are to some extent misaligned. They fly with a constant, trimmed angle of attack and a constant turn rate. Equations (27) show that, apart from an amplication factor $1/(1 - q/q_{\text{div}})$, this behavior is qualitatively unmodified

†Having solved Eq. (24) for η_∞, χ_∞, and α_∞ assume $q_{\text{div}} \simeq q_h$ and use Eqs. (1), (2), (4), (4a), (5a–c), (7a), (7c–k), (10a,b), (11a), (15b) and (19a). Also use $\lambda_N + \lambda_T = c_N + c_T = 1$ and $Q = \rho U^2/2$.

Table 1 Vehicle A (upper) and vehicle B (lower) distributed properties[a]

Station, m	Flexural beam stiffness, EI, 10^6 N · m^2	Mass per unit length, kg/m	c_{l_α},[b] m^{-1}
0.0	1.0	30	0.000
0.4	1.0, 0, 1.5	30, 60	—
0.5	—	60, 14	—
2.7	—	14, 62	—
2.8	1.5, 0, 0.4	62, 20	0.217
2.9	—	20, 30	—
3.4	—	—	0.573
3.9	—	30,20	2.165
4.0	0.4, 0, 0.2	—	3.820
4.1	—	20, 10	—
5.0	0.2	10	0.000
0.0	1.0	30	0.000
0.4	1.0, 0, 1.5	30, 60	—
0.5	—	60, 14	—
2.0	—	—	0.350
2.7	—	14, 62	—
2.8	1.5, 0, 0.25	62, 12	0.859, 6.366
2.9	0.25, 0.20	12, 18	4.775, 0.000
3.4	—	—	0.000
4.0	—	18, 12	0.159
4.5	0.20, 0, 0.10	12, 6	2.515, 4.106
5.0	0.10	6	0.000

[a]Multiple-valued entries correspond to discontinuities. Intermediate values are obtained by linear interpolation. See also Fig. 5.
[b]Coefficient of lift-slope per unit-length, referred to S_r.

by flexibility. The significance of q_{div} lies in the mathematical unboundedness of acceleration and deformation. Actually, however, either moderating nonlinear effects or structural failure must occur at substantially lower dynamic pressures. The analogy to imperfect column buckling is evident.

Conversion of Actual Lift Distributions

To apply the present theory to actual, distributed-lift vehicles, one must somehow choose points N and T and determine appropriate $C_{L_{\alpha_N}}$ and $C_{L_{\alpha_T}}$. The theory so far presented has no preference to any particular method of obtaining these quantities; yet results such as q_{div} are strongly sensitive to their values. It therefore should be understood that successful application of the theory depends not only on its own merits, but also, crucially, on the method used to convert actual distributions into pairs of concentrated lift-slopes. The method proposed here involves, for convenience, the lift distribution only, and is based on conserving its four lowest-order moments:

$$K_n \equiv \int_0^{l_e} x^n c_{l_\alpha}(x)\mathrm{d}x = x_N^n\, C_{L_{\alpha_N}} + x_T^n\, C_{L_{\alpha_T}}$$

$$n = 0,1,2,3 \qquad (28)$$

(For notation, see Fig. 2.) Equations (28) constitute a system in the unknowns x_N, x_T, $C_{L_{\alpha_N}}$, and $C_{L_{\alpha_T}}$. They guarantee the conservation, upon conversion, of the total lift and pitching moment coefficients, for all rigid-body modes as well as for bending modes with shapes expressible by, at most, a cubic polynomial. Solving them we obtain

$$l = \frac{\sqrt{K_0^2K_3^2 + 4K_1^3K_3 + 4K_0K_2^3 - 3K_1^2K_2^2 - 6K_0K_1K_2K_3}}{K_0K_2 - K_1^2} \qquad (29a)$$

$$x_N + x_T = (K_0K_3 - K_1K_2)/(K_0K_2 - K_1^2) \qquad (29b)$$

and the rest follow easily.

Table 2 Vehicle A (upper) and vehicle B (lower) concentrated quantities

Station, m	Quantity	Value
0.0 0.4	Concentrated lift-slope coefficients[a]	1.910
0.4 2.8 4.0	Structural joints stiffnesses	0.6×10^6 N·m/rad
0.0 0.4	Concentrated lift-slope coefficients[a]	1.910
0.4 2.8 4.0	Structural joints stiffnesses	0.60×10^6 N·m/rad 0.18×10^6 N·m/rad 0.30×10^6 N·m/rad

[a]Referred to S_r.

Table 3 Selected parameters calculated for vehicles A and B

Parameter	Vehicle A	Vehicle B
m	100.0 Kg	85.00 Kg
x_{cg}[a]	2.361 m	2.152 m
j_0^2	0.1313	0.1342
l	3.894 m	3.862 m
λ_N	0.4536	0.5288
λ_T	0.5464	0.4712
C_{L_α}	7.101	6.953
c_N	0.4374	0.3560
c_T	0.5626	0.6440
h_0	0.1090	0.1153
r_0^2	0.2580	0.2425
γ_{11}	2.357×10^{-2}	2.991×10^{-2}
γ_{21}	-1.486×10^{-2}	-1.583×10^{-2}
γ_{12}	-2.351×10^{-4}	-2.423×10^{-3}
γ_{22}	4.148×10^{-4}	-1.243×10^{-3}
μ	667.3	571.9
S_r	3.142×10^{-2} m^2	3.142×10^{-2} m^2
$(EI)_r$	3.333×10^5 N· m^2	1.926×10^5 N· m^2

[a]Measured from extreme aft.

We conclude by pointing out an interesting property of the pair (x_N,x_T),

$$\int_0^{l_e} (x - x_N)(x - x_T)c_{l_\alpha}(x)\,\mathrm{d}x = 0 \qquad (30)$$

which exposes it as a sort of "double" center of pressure. It is also possible to define a quantity σ, akin to statistics "standard deviation," which constitutes a measure of the deviation of $c_{l_\alpha}(x)$ from the model of two concentrated lift-slopes:

$$\sigma_4 = \frac{180}{l_e^4 C_{L_\alpha}} \int_0^{l_e(x - x_N)^2} \cdot (x - x_T)^2 c_{l_\alpha}(x)\,\mathrm{d}x \qquad (31)$$

The vanishing of σ thus defined is a necessary and sufficient condition for the aerodynamic load to be of the (x_N, x_T)-two-concentrated-forces type. A uniformly distributed $c_{l_\alpha}(x)$ makes $\sigma = 1$.

Numerical Examples

Extensive numerical tests were carried out[10] in order to establish present theory performance and limits of validity. Two examples, designated vehicle A and vehicle B, defined in Tables 1 and 2 and in Fig. 5, are presented here. Vehicle B is, in fact, a "3L" rather than "2L" configuration. It is included for the purpose of demonstrating the power of the theory to cope with even this, seemingly unfit, case. Table 3 brings selected parameters calculated for the two vehicles. In addition, examples for which actual divergence data exist (Jabiru sounding rockets[1,11]) are presented in Figs. 6 and 7. They show remarkably good agreement for 3L's.

Beside experimental results, comparisons are made with results of Ref. 9 method. That method uses a refined finite-element procedure to obtain four natural vibration modes and two rigid-body modes, together with their generalized masses, stiffnesses, and aerodynamic matrices. The 6 × 6 modal system then undergoes a numerical, dynamic stability root-locus analysis. Only frequency-domain characteristics are available for comparison. Reference 9 method is superior to the present one in two respects: 1) it treats the aerodynamic loads rigorously, without resort to conversion, and 2) it takes proper account of inertial loads associated with deformation acceleration.

We are interested in separating the error of the present method relative to that of Ref. 9 into two parts, each associated with one of the above sources. The reason is that only the second one constitutes a source of error inherent in the theory, whereas the first reflects only on the conversion method. To this end three calculations have been made for each vehicle: 1) pure present-theory; 2) conversion, then Ref. 9 method, and 3) pure Ref. 9 method.

Table 4 summarizes selected results and relative errors. It is seen that, as far as dynamic pressures are concerned, the total error is dominated by the conversion error. That incurred by assumption 4 is by far smaller and, from an engineering standpoint, insignificant. Note also that current theory results are conservative. Most striking are, however, the reasonably good results obtained for 3L-configured vehicle B.

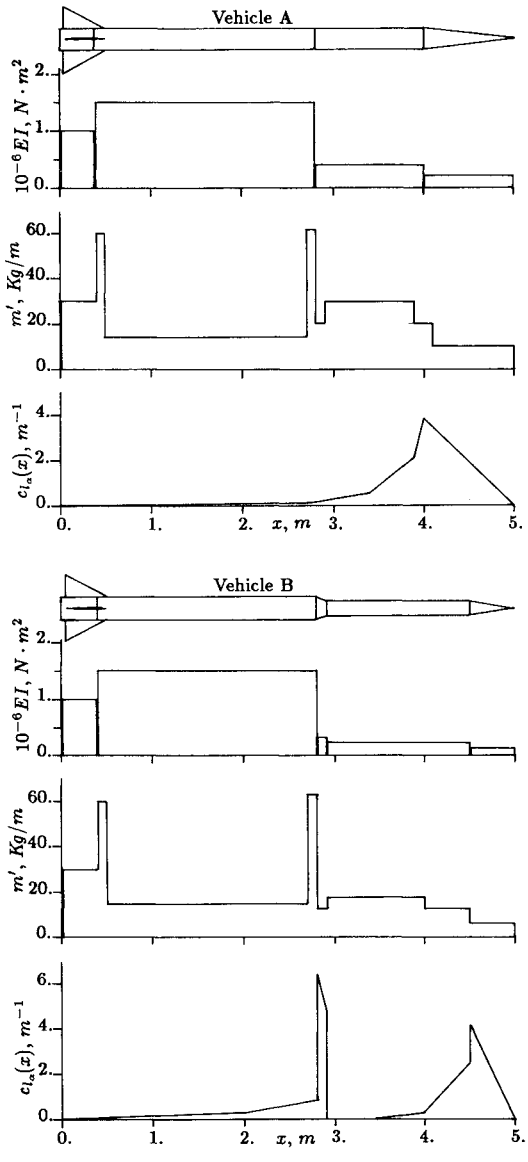

Fig. 5 Vehicle A (upper) and vehicle B (lower) distributed properties.

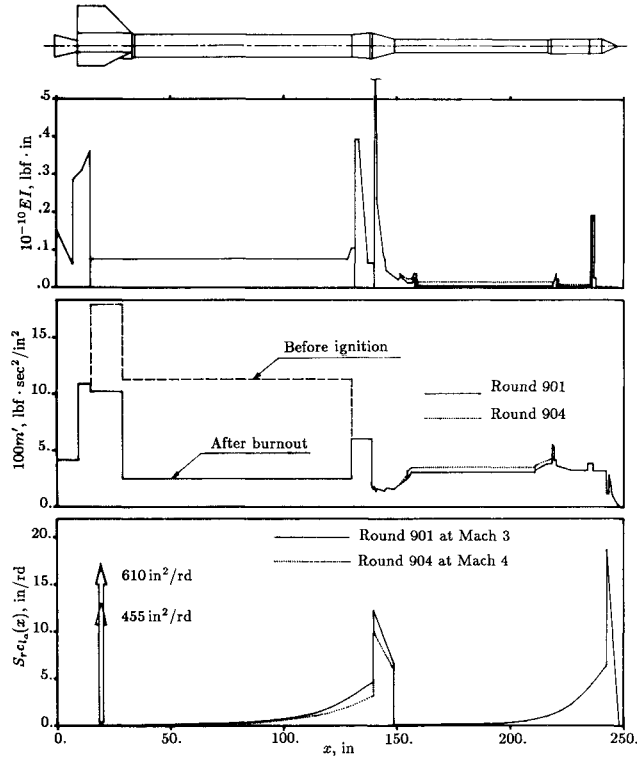

Fig. 6 Jabiru vehicles (Rounds 901 and 904) distributed properties.[1,11]

Table 4 Selected results and comparison with Ref. 9 method

Vehicle		q_{div}	q_h	q_D	$-100s_{\text{div}}^{(2)}$	$-100s_h^{(1)}$	$-100s_h^{(2)}$	$-100s_D$	$100\omega_{½}$[b]
A	(I) Present method	1.643	1.624	1.622	1.527	0.5444	0.9835	0.7640	4.673
	(II) Ref. 9, converted	1.631	1.611[a]	1.610	1.488	0.5603[a]	0.9288[a]	0.7446	4.656
	(III) Pure Ref. 9	1.723	1.702[a]	1.701	1.517	0.5576[a]	0.9604[a]	0.7591	4.690
	Assump. 4 error, I:II, %	0.8	0.8	0.7	2.6	−2.8	5.9	2.6	0.4
	Total error, I:III, %	−4.6	−4.6	−4.7	0.7	−2.4	2.4	0.6	−0.4
B	(I) Present method	1.600	1.581	1.579	1.727	0.6110	1.116	0.8634	5.169
	(II) Ref. 9, converted	1.579	1.561[a]	1.559	1.700	0.6179[a]	1.083[a]	0.8504	5.168
	(III) Pure Ref. 9	1.811	1.791[a]	1.788	1.755	0.5787[a]	1.176[a]	0.8775	5.253
	Assump. 4 error, I:II, %	1.3	1.3	1.3	1.6	−1.1	3.0	1.5	0.0
	Total error, I:III, %	−11.7	−11.7	−11.7	−1.6	5.6	−5.1	1.6	−1.6

[a]The method of Ref. 9 does not yield q_h directly. The values appearing here were obtained as $\lim_{\mu\to\infty} q_{\text{div}}$. [b]$\omega_{½}$ = Nondimensional short-period frequency for $q/q_{\text{div}} = ½$.

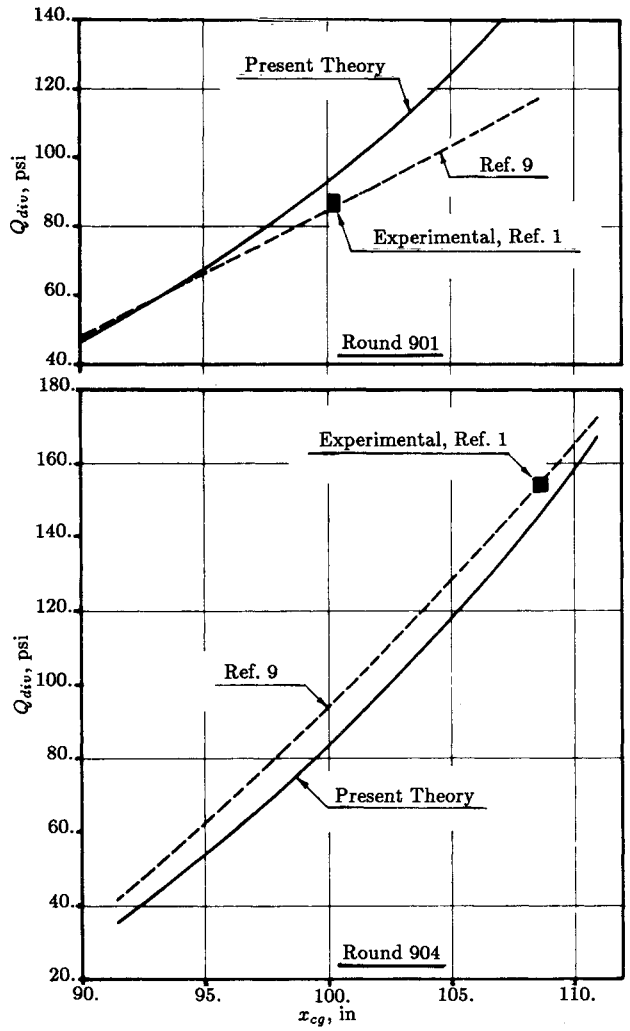

Fig. 7 Jabiru vehicles divergence data[1] and theoretical predictions.

Concluding Remarks

The phenomenon of rocket vehicles aeroelastic divergence, as related to configurations having only nose and tail aerodynamic lateral forces, has been modeled and investigated in closed form. Notable results are the flexibility influenced short-period mode equations of motion, Eqs. (8), (12), and (26); the divergence dynamic pressure and its approximation, Eqs. (17) and (19); the generalized static margin, Eqs. (18) and (20); and the divergence steady-state motion, Eqs. (25) and (27). Application to distributed-lift vehicles is made possible by means of Eqs. (28) and (29).

Considerable simplification arises in general divergence analyses if, in addition to employing assumption 4, certain results of this work are assumed a priori. They are: 1) the unimportance of transverse velocity terms in the aerodynamic forces, which merely cause a slight offset between q_{div}, q_h, and q_D and 2) the existence in divergence of a static trim condition, $\ddot{\theta} = 0$, $M = 0$ (Eqs. 25b and c). Using these, the general ROVALD problem can be reduced to an elementary algebraic one in α and $U\dot{\gamma}$.

The results obtained here highlight the essentials of ROVALD and the features responsible for it: mass, stiffness, and lift-slope distributions such that lateral-translational acceleration, maintained by aerodynamic forces, bends the vehicle into a shape which increases the nose angle of attack relative to that of the tail. Divergence-prone configurations are those having most of their mass and flexibility distributed inward of the main lift-slope localities. These include all typical rocket vehicle configurations as well as some flexible canard flight vehicle ones.

In the introduction to this paper the idea of the concentrated lift-slope pair is presented as an intuitive approximation to a 2L-type $c_{l_\alpha}(x)$ distribution. We are now in a position to propose a radical change in this view, namely, that for any divergent vehicle, 2L or not, there exists such a pair, which constitutes an *equivalent*—with respect to short-period and divergence behavior—of the actual $c_{l_\alpha}(x)$; it is defined as the pair conserving C_{L_α}, C_{M_α}, C_{M_q}, and q_{div}. (Since h is the dominant factor in the decreasing of both static stability and short-period frequency it is believed that the q_{div}-conserving pair will also fairly well conserve short-period frequency, provided the latter is sufficiently separated from the first bending frequency.) If q_{div} is known in advance then this equivalent can be determined exactly, by some iterative method involving Eq. (17); or else, an approximation of it must be sought, using conversion methods such as those presented here. With this in mind the present model acquires a far greater generality than has initially been possible to presume.

References

[1]Thomson, K. D., "The Aero-Elastic Divergence of Slender Multi-Stage Test Vehicles," Weapons Research Establishment, Salisbury, South Australia. TN HSA 93, Nov. 1962.

[2]Meyers, S. C., "Aeroelastic Analysis of Sounding Rocket Vehicles," AIAA 3rd Sounding Rocket Technology Conference, AIAA Paper 73-284, March 1973.

[3]Matejka, D. Q., "Aeroelastic Bending of a Sounding Rocket Vehicle," AIAA 2nd Sounding Rocket Technology Conference, AIAA Paper 70-1400, Dec. 1970.

[4]O'Keefe, D. A., "General Static Aeroelastic Analysis for a Body of Revolution," *AIAA Journal*, Vol. 3, Dec. 1965, pp. 2256–2261.

[5]Alley, V. L. and Harper-Gerringer, A., "An Analysis of Aeroelastic Divergence in Unguided Launch Vehicles," NASA TN D-3281, March 1966.

[6]Young, C. P., "A Numerical Method for Determining the Aeroelastic Divergence Characteristics of Unguided, Slender-Body, Multistage Launch Vehicles," NASA TN D-3893, April 1967.

[7]Booth, A. W., "A Generalized Analysis of Aeroelastic Bending of a Slender-Body, Non-Uniform Flight Vehicle," Fairchild-Hiller/NASA Rept. ER 106, April 1967.

[8]Glasson, A. R. and Pearson, K. G., "A FORTRAN II Computer Program for Steady-State Aeroelastic Evaluation of Slender, Non-Rolling Rocket Vehicles," Weapons Research Establishment, Salisbury, South Australia, TN HSA 128, Oct. 1967.

[9]Elyada, D., "A Computer Program for Calculating Aeroelastic Divergence of Unguided Rocket Vehicles," Israel Armament Development Authority, Haifa, TM 2147/1975, May 1975 (in Hebrew).

[10]Elyada, D., "Closed-Form Analysis of the Aeroelastic Divergence Characteristics of Flexible, Unguided, Non-Spinning Rocket Vehicles Having Two Lift-Producing Components," M.Sc. Thesis, Technion – Israel Institute of Technology, Haifa, July 1977 (in Hebrew).

[11]Young, C. P., "Analysis of the Aeroelastic Divergence of Two Experimental, Unguided Launch Vehicles," NASA TN D-4846, Nov. 1968.